ACS Catalysis

Research Article

Cite This: ACS Catal. 2018, 8, 10486−10497

pubs.acs.org/acscatalysis

Kinetic Fingerprints of Catalysis by Subsurface Hydrogen

Irem Sen[†] and Andrew J. Gellman*[,†,‡]

[†]Department of Chemical Engineering, Carnegie Mellon University, Pittsburgh, Pennsylvania 15213, United States

[‡]W. E. Scott Institute for Energy Innovation, Carnegie Mellon University, Pittsburgh, Pennsylvania 15213, United States

Supporting Information

ABSTRACT: Mechanisms for catalytic H_2-D_2 exchange involving subsurface hydrogen, H′ (D′), have been analyzed to predict the ranges of reaction conditions over which the reaction orders, n_{H_2} and n_{D_2}, can be used to distinguish among the various possible mechanisms. Four different mechanisms and combinations thereof have been considered: a Langmuir−Hinshelwood (LH) model, a breakthrough model invoking direct reaction between surface H(D) and subsurface H′ (D′), and two models invoking activation of H (D) by H′ (D′). In parallel, the kinetics of H_2-D_2 exchange have been measured over 90 Ag_xPd_{1-x} alloy film samples with a continuous range of compositions: $x = 0 \rightarrow 1$. For conditions with $P_{H_2} \gg P_{D_2}$, the reaction orders are found to be $n_{H_2} \cong 0$ and $n_{D_2} \cong 1$. The value of $n_{H_2} \cong 0$ is inconsistent with an LH mechanism under conditions with a hydrogen coverage of $\theta \cong 1$. A mechanism in which two subsurface H′ (D′) atoms promote recombinative desorption of H (D) atoms on the surface is consistent with the observed reaction orders under conditions in which the coverages on the surface and in the subsurface are $\theta \cong 1$ and $\theta' \approx 0$, respectively.

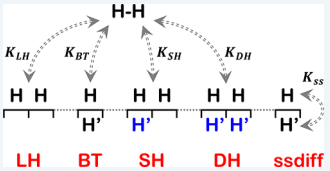

KEYWORDS: *kinetics, catalysis, silver, palladium, alloy, H_2-D_2 exchange, hydrogen adsorption, subsurface hydrogen*

1. INTRODUCTION

The ability of transition metals to adsorb H_2 dissociatively on their surfaces, absorb H atoms into their subsurface, and allow H atom diffusion through their bulk makes them attractive for many applications such as hydrogen storage, hydrogen purification, and heterogeneous catalysis of many hydrogenation, dehydrogenation, and hydrogenolysis reactions.[1−5] For the most part, the framework for thinking about heterogeneous catalytic processes involving hydrogen has been that of Langmuir and Hinshelwood, in which adsorbed H atoms reside and react on the metal surface.[6,7] However, recently, H′ atoms absorbed into the metal subsurface have been shown to play a very important role in heterogeneous catalysis,[8,9] particularly in the hydrogenation of alkenes and alkynes on metals such as Pd and Ni.[10−18] Consequently, both surface hydrogen (herein H) and subsurface hydrogen (herein H′) must be considered in describing the kinetics of catalytic reactions involving hydrogen transfer. Herein, we develop a framework for describing the catalytic kinetics of H′ reacting via several mechanisms and apply this framework to understanding the kinetics of H_2-D_2 exchange ($H_2 + D_2 \rightarrow 2HD$) on Ag_xPd_{1-x} alloys.

Ag_xPd_{1-x} alloys are commonly used as catalysts for the hydrogenation of alkynes and alkenes[19−21] and as solid permeation membranes for the purification of hydrogen from gas streams.[22−25] Numerous studies of H_2 on Pd surfaces have shown that it adsorbs with a negligible barrier to dissociation and a high heat of adsorption[26−28] and that it can be sorbed into the subsurface.[29−31] In contrast, H_2 does not adsorb dissociatively onto Ag surfaces at room temperature and its adsorption has been predicted to be endothermic.[32−35] Nonetheless, alloying Ag with Pd yields hydrogen purification membranes and hydrogenation catalysts that are superior to pure Pd.[19,20,23,36−39]

The importance of subsurface H′ in metallic catalysts is becoming increasingly well documented.[8,9,12,20,27,35,39,40] Recent studies using DFT have shown that H′ in the first subsurface layer is much less stable than H adsorbed on the surface.[27] Among the transition metals, Pd is the only one in which subsurface H′ atoms are energetically favorable with respect to gaseous H_2.[7,35] In order to model the kinetics of catalytic reactions on Pd and Pd-based alloys, the contribution of subsurface H′ must be considered. In this work, we provide kinetic evidence for the participation of subsurface H′ in the H_2-D_2 exchange reaction occurring on Pd−Ag alloy catalysts. More importantly, we have developed a framework for describing the kinetics of several postulated mechanisms that involve both surface H (D) and subsurface H′ (D′).

The H_2-D_2 exchange reaction on Pd(111) and Pd nanoparticles has been studied recently by Savara et al. using molecular beam measurements of the catalytic reaction kinetics.[8,9] At temperatures in the range 200−300 K and under conditions in which $P_{D_2} \gg P_{H_2}$, they observed that the reaction order in P_{D_2} was $n_{D_2} = 0$, inconsistent with Langmuir−Hinshelwood (LH) kinetics that predict $n_{D_2}^{LH} = -1$ for $P_{D_2} \gg P_{H_2}$ and high total coverage, $\theta \cong 1$. At temperatures >300 K in Savara's work, the reaction order was consistent with LH kinetics. They suggested that a mechanism involving participation of subsurface H′ is active in the low-temperature regime. Direct evidence for the presence of subsurface H′ and its participation in the H_2-D_2 exchange reaction was obtained from experiments using nuclear

Received: June 4, 2018
Revised: September 17, 2018
Published: September 24, 2018

DOI: 10.1021/acscatal.8b02168
ACS Catal. 2018, 8, 10486−10497

reaction analysis.[41] Studies of other catalytic processes including ethylene and acetylene hydrogenation on Pd and Pd−Ag alloys have implicated subsurface H′ in the reaction mechanism and the resulting kinetics.[20,42]

In this study, the kinetics of the H_2-D_2 exchange reaction have been measured on Ag_xPd_{1-x} films with compositions spanning $x = 0 \rightarrow 1$ over a wide range of reaction conditions: T = 333−593 K, P_{H_2}= 30−3 kPa, and P_{D_2}= 30−0.03 kPa. Consistent with the aforementioned work,[8,9] our data show that the reaction order in P_{H_2} is $n_{H_2} = 0$ when $P_{H_2} \gg P_{D_2}$, inconsistent with a LH mechanism. In order to rationalize the observed kinetics, we have solved, in closed form, four kinetic models involving subsurface H′ (D′) in the H_2-D_2 exchange mechanism. We demonstrate that a mechanism in which two subsurface H′ (D′) atoms promote recombination of two H (D) atoms on the surface is consistent with the observed value of $n_{H_2} = 0$ when $P_{H_2} \gg P_{D_2}$.

2. EXPERIMENTAL SECTION

The catalytic reaction kinetics for H_2-D_2 exchange were measured on Ag_xPd_{1-x} composition spread alloy films (CSAF) at 90 locations having different compositions in the range $x = 0 \rightarrow 1$.

2.1. CSAF Preparation. The CSAF samples were prepared by evaporative deposition of Pd and Ag onto a 14 × 14 × 2 mm^3 polished Mo substrate (Valley Design Corp.) using a rotatable shadow mask CSAF deposition tool that has been described in detail previously.[43] Mo was chosen as a substrate material because it does not alloy with Ag or Pd at the annealing and reaction temperatures.[44−47] The deposition rates from the Pd and Ag electron beam evaporation sources were controlled independently by the heating power and calibrated using a quartz crystal microbalance. The film thickness (∼100 nm in this work) was controlled by the deposition time. The positions and orientations of the shadow masks between the sources and the substrate resulted in opposing flux gradients of Pd and Ag across the substrate. CSAFs were deposited and then annealed (800 K for 1 h) under ultrahigh-vacuum conditions (UHV). These conditions are sufficient to induce film crystallization.[45,48]

2.2. Characterization of CSAF Composition. XPS analysis of the Ag_xPd_{1-x} CSAF was performed in a ThetaProbe instrument (Thermo-Fisher Scientific Inc.) to map the local composition across the sample surface. The CSAF sample can be positioned by an automated stage in the ThetaProbe, allowing composition analysis at a set of predetermined points. Spatially resolved maps of the Ag $3d_{5/2}$ and Pd $3d_{3/2}$ XP spectra were obtained by lateral translation of the CSAF with its plane intersecting the source-analyzer focal point. The X-ray spot size was ∼200 μm in diameter. The pass energy of the hemispherical energy analyzer was set to 40 eV. Atomic fractions of the components were estimated using the Avantage Data System software package, which contains a library of the binding energies and the relative intensities of XPS features from the pure metals.

2.3. Measurement of H_2-D_2 Exchange Kinetics. The H_2-D_2 exchange activity of the Ag_xPd_{1-x} CSAFs was measured using a high-throughput 100-channel microreactor array which has been described in detail elsewhere.[49] Reactants were continuously delivered to 100 isolated regions of the Ag_xPd_{1-x} CSAF surface, and products were continuously withdrawn from each region for analysis using an Extrel quadrupole mass spectrometer. For this specific study, only 90 channels of the reactor were in use because the inlet to 1 row of 10 reactors was blocked. Hence, only 90 different catalyst compositions were studied across the Ag_xPd_{1-x} CSAF.

The Ag_xPd_{1-x} alloy composition dependent H_2-D_2 exchange activity of Ag_xPd_{1-x} CSAF was measured at atmospheric pressure and over a temperature range from 333 to 593 K. The H_2 inlet partial pressures spanned the range $P^{in}_{H_2}$ = 3.04−30.4 kPa and the D_2 inlet partial pressures spanned $P^{in}_{D_2}$ = 0.03−30.4 kPa with Ar constituting the remainder of the gas flow. The temperature was increased in 20 K increments, and the reaction was allowed to reach steady state by waiting for 4 min at each temperature before beginning the analysis of the product gases from each of the 100 reactor channels.

The composition of the reaction products was calculated by assuming that the mass spectrometer signals at m/z = 2, 3, and 4 amu obtained from the product gas samples were proportional to the H_2, HD, and D_2 partial pressures. Baseline (0% conversion) signals at m/z = 2, 3, and 4 amu were collected by sampling the feed gas mixture directly without it contacting the CSAF surface. Note that at equilibrium, the composition of the product gases is given by

$$\frac{P_{HD}^2}{P_{H_2}P_{D_2}} = 4.16 \exp\left(\frac{-77.7}{T}\right) \quad (1)$$

where P_{H_2}, P_{D_2}, and P_{HD} are the partial pressures of H_2, D_2, and HD, respectively, and T has units of K.[50] Thus, the reaction mixture never reaches 100% conversion of H_2 and D_2 into HD.

3. RESULTS

3.1. Characterization of CSAF Composition. The near-surface composition of the Ag_xPd_{1-x} CSAF was mapped by X-ray photoelectron spectroscopy (XPS) as a function of position on the Mo substrate using a 13 × 13 grid with 1 mm spacing. Although the CSAF is deposited onto a 14 × 14 mm^2 Mo substrate, the region of interest is the 10 × 10 mm^2 area spanned by the 10 × 10 array of microreactors. The composition map of the area on the CSAF used for the measurement of catalytic reaction kinetics is shown in Figure 1. The CSAF has been

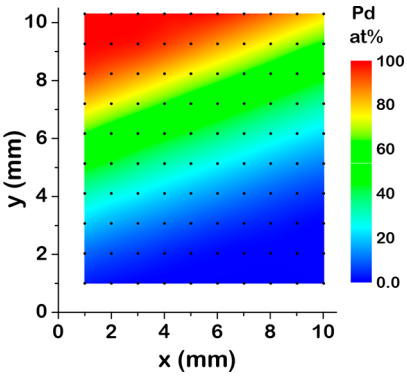

Figure 1. Pd composition (measured by XPS) versus position on the Ag_xPd_{1-x} binary CSAF. Black dots represent XPS measurement points.

deposited such that the iso-composition lines are oriented at an angle with respect to the edge of the substrate which is aligned with the microreactor array. This tilted configuration of the CSAF ensures that each channel of the microreactor samples a different alloy composition. In the region sampled by the

DOI: 10.1021/acscatal.8b02168
ACS Catal. 2018, 8, 10486−10497

microreactor array, the Ag_xPd_{1-x} CSAF spanned the composition range $x = 0 \rightarrow 1$.[43,51]

3.2. H_2–D_2 Exchange Activity on Ag_xPd_{1-x} CSAF. H_2–D_2 exchange kinetics over the Ag_xPd_{1-x} CSAF were measured by feeding H_2, D_2, and Ar mixtures into the microreactor at a constant temperature, partial pressure, and flow rate while monitoring the product gas composition by mass spectrometry. Mass spectrometer signals were used to calculate conversion, X_{H_2}, for 90 different Ag_xPd_{1-x} compositions, x, at 14 different temperatures, T = 333–593 K, and 14 different flow conditions (see Supporting Information section 1, Table S1). The Ag_xPd_{1-x} binary CSAF displayed stable activity during the course of the experiments. Plots of X_{H_2} versus T for all 90 different Ag_xPd_{1-x} compositions are given in Figure 2 for one

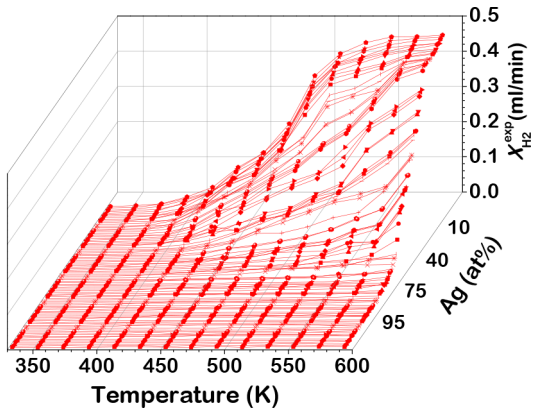

Figure 2. H_2 conversion, X_{H_2}, versus T measured across Ag_xPd_{1-x} composition space. The inlet flow conditions in each channel were as follows: P_{tot} = 1 bar, $F^{in}_{H_2} = F^{in}_{D_2}$ = 0.10 mL/min, and F^{in}_{Ar} = 0.13 mL/min ($P^{in}_{H_2} = P^{in}_{D_2}$ = 30 kPa).

inlet flow condition ($F^{in}_{H_2} = F^{in}_{D_2}$ = 0.10 mL/min/channel and F^{in}_{Ar} = 0.13 mL/min/channel) at a total pressure of 1 bar. Similar data are provided in Supporting Information section 2 for all 14 reaction conditions. Across the CSAF, H_2–D_2 exchange activity increases with increasing T and decreasing Ag content, x, for all different inlet conditions.

3.3. Reaction Order for H_2–D_2 Exchange on Ag_xPd_{1-x}. The pressure dependence of the H_2–D_2 exchange rate over Ag_xPd_{1-x} alloys has been investigated across the temperature range T = 333–593 K by varying the inlet partial pressures $P^{in}_{H_2}$ and $P^{in}_{D_2}$ independently and measuring the outlet HD flow rate, F^{out}_{HD}. Figure 3a (dashed lines and colored symbols) shows the HD production rate versus $P^{in}_{D_2}$ with $P^{in}_{D_2} \ll P^{in}_{H_2}$ = 30.4 kPa measured at T = 413 K on five different Ag_xPd_{1-x} compositions. Figure 3a (solid lines and black symbols) also shows the HD production rate on an alloy with x = 0.01 at five temperatures in the range T = 333–413 K. Figure 3b shows the HD production rate versus $P^{in}_{H_2}$ with $P^{in}_{H_2} \gg P^{in}_{D_2}$= 0.03 kPa for five alloy compositions and over the temperature range T = 333–413 K. Under all of these conditions, the conversion of D_2, the limiting reagent, was <10%. When $P^{in}_{H_2} \gg P^{in}_{D_2}$, the reaction order with respect to $P^{in}_{D_2}$ is n_{D_2} = 0.92, close to the first-order behavior predicted by LH kinetics. In contrast, the reaction order in $P^{in}_{H_2}$ when $P^{in}_{H_2} \gg P^{in}_{D_2}$ is n_{H_2} = 0.01, consistent with the measurements of previous studies[8,9] and inconsistent with classical LH kinetics at high hydrogen coverages. With $P^{in}_{H_2} \gg P^{in}_{D_2}$, reaction orders of $n_{D_2} \cong 1$ and $n_{H_2} \cong 0$ were observed for all alloy compositions (x = 0–0.9) and temperatures (T = 333–413 K) at which conversions could be measures in the range $0.1 < X_{D_2} < 0.0001$.

LH kinetics predict that under low-pressure conditions at which the coverages are $\theta_D \ll \theta_H \ll 1$, the reaction orders should be $n_{H_2} = 0$ and $n_{D_2} = 1$, as we observe; however, at the pressures used, the coverage ought to be $\theta \approx 1$. This is supported by estimates in the next section that the hydrogen adsorption equilibrium constant ranges in value from $K_{LH} = 3 \times 10^{-1}$ to 3×10^{-3} Pa^{-1} over the range T = 333–413 K. In combination with $P^{in}_{H_2}$ = 30 kPa, this leads to high coverages of adsorbed hydrogen, $\sqrt{K_{LH}P^{in}_{H2}} \gg 1$. When $P^{in}_{H_2} \gg P^{in}_{D_2}$ and $\theta_D \ll \theta_H \approx 1$, the LH reaction orders should be $n_{H_2} = -1$ and $n_{D_2} = 1$. The data in Figure 3 are clearly indicative of a mechanism other than LH.

4. DISCUSSION

In the following, we explore the kinetic consequences of several reaction mechanisms involving H′ in the immediate subsurface layer, in order to reconcile the reaction orders observed in our experiments on Ag_xPd_{1-x} alloy surfaces (Figure 3) and those observed using molecular beam experiments on the Pd(111) surface and on supported Pd nanoparticles.[8] The key observation that $n_{H_2} = 0$ for $P^{in}_{H_2} \gg P^{in}_{D_2}$ and under conditions in which the total coverage of H and D atoms is expected to be $\theta \approx 1$ suggests that the mechanism is not a simple LH process. Zero-order kinetics in LH surface reaction mechanisms are often associated with conditions under which the coverage of a reactant species saturates the surface, $\theta \approx 1$, and is insensitive to increases in that reactant partial pressure.[4] However, for bimolecular reactions in which two reactants are competing for adsorption sites, increasing the pressure of the high coverage reactant with $\theta \approx 1$ results in displacement of the low-coverage reactant and, therefore, a negative reaction order with respect to the partial pressure of the high coverage species. This type of negative-order kinetics predicted by the LH mechanism is clearly not observed in H_2–D_2 exchange kinetics on our surfaces.

In the following, we consider the kinetic consequences on H_2–D_2 exchange of the five processes illustrated in Figure 4 and combinations thereof. At the left is the classical LH process in which gas-phase H_2, HD, and D_2 are equilibrated with H and D atoms adsorbed on the surface. We use the standard LH assumptions of zero or one atom per site and no interactions between adsorbates. In addition, we ignore isotope effects on the adsorption equilibrium constant, K_{LH}, and on the adsorption and desorption rate constants, k^{LH}_a and k^{LH}_d. The breakthrough (BT) mechanism is one in which dissociative adsorption of H_2 leads directly to one H atom on the surface and an H′ atom in the immediate subsurface. Equivalently, H_2 desorption results from direct recombination of a surface H with a subsurface H′. In the single-subsurface hydrogen (SH) activation mechanism, H_2 adsorbs and desorbs preferentially from adjacent sites on the surface having one H′ atom in one of the two subsurface sites. The H′ is colored blue in Figure 4 to indicate that it does not participate directly in the reaction. In the dual-subsurface hydrogen (DH) activation mechanism H_2 adsorbs and desorbs preferentially from adjacent sites on the surface having H′ atoms in both of the subsurface sites. Finally, at the right of Figure 4 we depict a diffusion process by which H and H′ atoms are

DOI: 10.1021/acscatal.8b02168
ACS Catal. 2018, 8, 10486–10497

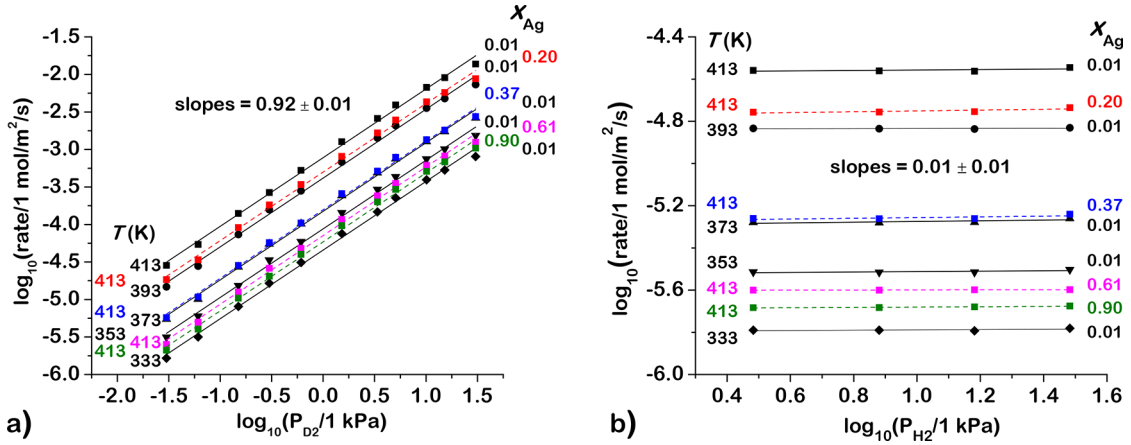

Figure 3. (a) HD production rates on five different Ag_xPd_{1-x} compositions and at five different temperatures plotted versus P_{D_2} with $P_{D_2} \ll P_{H_2} = 30.4$ kPa. The reaction orders are all $n_{D_2} \cong 1$. (b) HD production rates on five different Pd compositions and at five different temperatures as a function of P_{H_2} with $P_{H_2} \gg P_{D_2} = 0.03$ kPa. The reaction orders are all $n_{H_2} \cong 0$. The total conversions of the minority reaction component are all $X_{D_2} < 0.1$.

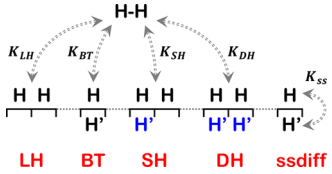

Figure 4. Surface−subsurface mechanisms for H_2 (and DH, D_2) dissociative adsorption and recombinative desorption during H_2−D_2 exchange: Langmuir−Hinshelwood (LH), breakthrough (BT), single-subsurface hydrogen (SH), and dual-subsurface hydrogen (DH). At the right we depict surface−subsurface diffusive (ssdiff) transport of H (D). The H′ atoms depicted in blue influence the adsorption and desorption kinetics but do not participate in the reaction.

exchanged between the surface and the subsurface sites. The key point is that under steady-state catalytic conditions these processes establish equilibria among H_2, D_2, and HD in the gas phase, H (D) adsorbed on the surface, and H′ (D′) absorbed into the subsurface.

The potential energy framework for considering the processes depicted in Figure 4 is shown in Figure 5. The free energy difference between gas-phase H_2 and two adsorbed H atoms, ΔE_{ads}, is given per atom. The free energy difference between a surface H (D) and a subsurface H′ (D′) is ΔE_{ss}. The LH, SH, and DH mechanisms all result in the adsorption of two atoms from the dissociative adsorption of H_2, D_2, or HD onto the surface. The only difference lies in the activation barriers, which are dictated by the number of H′ atoms in the subsurface: zero, one, and two for the LH, SH, and DH mechanisms, respectively. In keeping with the assumptions of the Langmuir model for adsorption, in which there are no interactions between adsorbed species (either on the surface or in the subsurface), the adsorption free energies are identical for the LH, SH, and DH models. The subsurface H′ influences the adsorption and desorption barriers and rate constants but not the adsorption energetics or equilibria; $K_{LH} = K_{SH} = K_{DH}$. This is probably a fairly good approximation under conditions in which the coverage of subsurface H′ and D′ is low, $\theta' \ll 1$, and therefore the average heat of adsorption across the surface is not significantly influenced by the subsurface H′. In section 4.6 we discuss the consequences of relaxing the assumption that $K_{LH} = K_{SH} = K_{DH}$ and demonstrate that it would not affect the reaction order $n_{H_2} = 0$ when $P^{in}_{H_2} \gg P^{in}_{D_2}$ and the total coverage on the active sites with subsurface hydrogen is still $\theta_H \approx 1$. The other key relationship implicit in Figure 5 is that $K_{LH} = K_{ss}K_{BT}$.

In the following four sections we describe the rate laws for catalytic HD production from mixtures of H_2 and D_2 in the gas phase as derived using the LH, LH+BT, SH+ssdiff, and DH +ssdiff models and standard steady-state assumptions for the coverages θ_H, θ_D, θ'_H, and θ'_D. Derivations of the rate laws are given in the Supporting Information for these four processes and for LH+ssdiff, pure BT, and BT+ssdiff processes. The notation "SH+ssdiff" implies a process involving both the SH mechanism for adsorption and desorption and the surface−subsurface diffusion process for transport of H into and H′ out of the subsurface.

In describing and thinking about the pressure regimes over which the H_2−D_2 exchange reaction adopts different reaction orders with respect to the inlet pressures $P^{in}_{H_2}$ and $P^{in}_{D_2}$ it is useful to understand how the adsorbate coverages θ, θ_H, θ_D, θ', θ'_H, and θ'_D scale with $K_{LH}P^{in}_{H_2}$, $K_{LH}P^{in}_{D_2}$, and K_{ss}. As will be shown, the adsorbate coverages under all scenarios have the same functional form.

$$\theta = \frac{K_{LH}P^{tot}}{\sqrt{K_{LH}P^{tot}} + K_{LH}P^{tot}} \quad \theta_H = \theta\frac{P^{in}_{H_2}}{P^{tot}} \text{ and } \theta_D = \theta\frac{P^{in}_{D_2}}{P^{tot}} \tag{2}$$

$$\theta' = \frac{K_{ss}K_{LH}P^{tot}}{\sqrt{K_{LH}P^{tot}} + K_{ss}K_{LH}P^{tot}}$$
$$\theta'_H = \theta\frac{P^{in}_{H_2}}{P^{tot}} \text{ and } \theta'_D = \theta\frac{P^{in}_{D_2}}{P^{tot}} \tag{3}$$

These coverages are plotted against $(K_{LH}P^{in}_{H_2}, K_{LH}P^{in}_{D_2})$ in Figure 6. For purposes of representing the subsurface concentrations, we have chosen to use $K_{ss} = 2.3 \times 10^{-4}$ at 413 K on the basis of the energy difference of 29 kJ/mol between H and H′ calculated on the Pd(100) and Pd(111) surfaces.[27] The coverage ranges from $\theta = 0$ (blue) to 1 (red) with a coverage of $\theta = 0.5$ indicated by green. In the lower left quadrant of $(K_{LH}P^{in}_{H_2}, K_{LH}P^{in}_{D_2})$ space both coverages are $\theta_H, \theta_D \ll 1$. In the upper right quadrant H and D are competing for adsorption sites. In the lower right quadrant $\theta_H \approx 0$ and $\theta_D \approx 1$ and in the upper left quadrant $\theta_D \approx 0$ and $\theta_H \approx 1$. With $K_{ss} = 2.3 \times 10^{-4}$ the subsurface H′ (D′) coverage remains low until $K_{LH}P^{in}_{H_2} = 10^7$ and/or $K_{LH}P^{in}_{D_2} = 10^7$.

DOI: 10.1021/acscatal.8b02168
ACS Catal. 2018, 8, 10486−10497

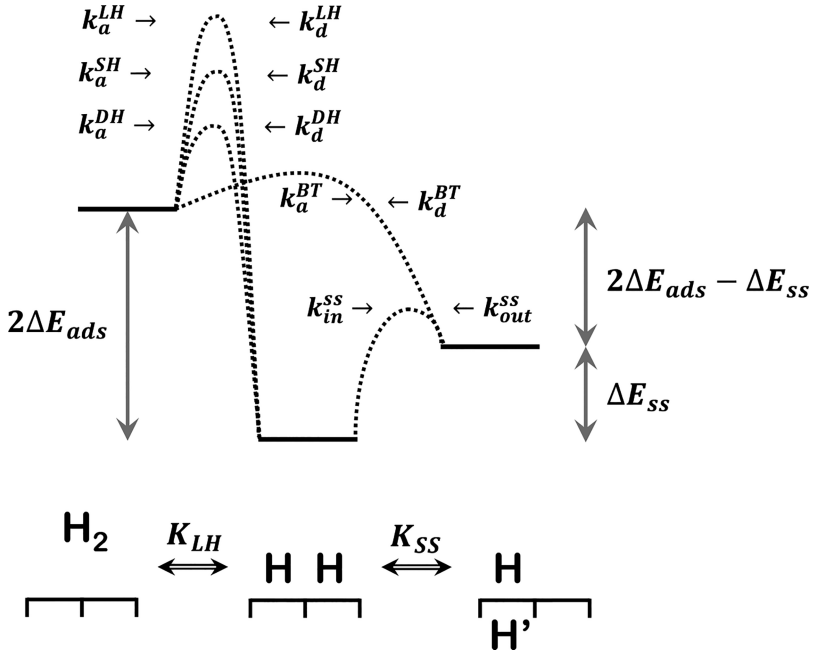

Figure 5. Potential energy diagram describing the equilibria and the kinetic barriers between relevant states: H_2 in the gas phase (left), two adsorbed H atoms (middle), and an H′ atom in the subsurface (right). The rate constants are k_a for H_2 adsorption, k_d for H_2 desorption, k_{in} for H atom surface to subsurface diffusion, and k_{out} for H atom subsurface to surface diffusion. The superscripts on the rate constants represent the four different H_2-D_2 exchange mechanisms: LH for Langmuir−Hinshelwood, BT for breakthrough, SH for single-subsurface H′ promotion, and DH for dual subsurface H′ promotion. The equilibrium constants are K_{LH} for H_2 adsorption and K_{ss} for surface H to subsurface H′ exchange.

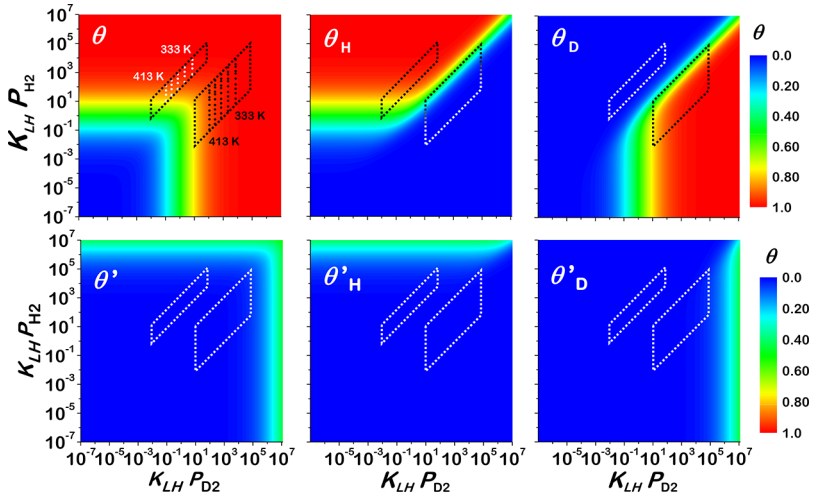

Figure 6. Adsorbate coverages θ, θ_H, θ_D, θ', θ'_H, and θ'_D versus $(K_{LH}P^{in}_{H_2}, K_{LH}P^{in}_{D_2})$. A value of $K_{ss} = 2.3 \times 10^{-4}$ was used to calculate the coverages of subsurface species. The points on the plot for θ mark the estimated values of $(K_{LH}P^{in}_{H_2}, K_{LH}P^{in}_{D_2})$ at which measurements were made on the basis of estimated values of $K_{LH} \approx 3 \times 10^{-3}$ to 3×10^{-1} Pa^{-1} over the temperature range 413−333 K. The parallelograms outline the regions in which measurements were made assuming a factor of $10^{\pm 1}$ uncertainty in K_{LH}.

On the plot of θ versus $(K_{LH}P^{in}_{H_2}, K_{LH}P^{in}_{D_2})$ in Figure 6 we have marked the points at which we have made measurements of the rates of H_2-D_2 exchange. These have required an estimate of the value of K_{LH} at temperatures in the range T = 333−413 K. These are based on measured values for the rate constants for dissociative adsorption and recombinative desorption of H_2 on Pd (α-hydride phase) during H_2-D_2 exchange.[52] The pre-exponential factors for dissociative adsorption and associative desorption are obtained from transition state theory as $\nu_{ads} = 10^{-4}$ mol/(m^2 s Pa) and $\nu_{des} = 10^6$ mol/(m^2 s), respectively.[53] For Pd, activation barriers for dissociative adsorption $\Delta E^{\ddagger}_{ads}$ = 0.12 eV and associative desorption $\Delta E^{\ddagger}_{des}$ = 0.68 eV were used.[52] The heat of adsorption of H on the Pd surface ($\Delta E_{ads} = \Delta E^{\ddagger}_{ads} - \Delta E^{\ddagger}_{des}$) used in this study is in good agreement with the values reported in the literature.[54−58] These yield an estimated range of $K_{LH} \approx 10^{-3}-10^{-1}$ over T = 413−333 K. Also on the coverage plots in Figure 6 we outline the two regions that contain our measurement points assuming a factor of $10^{\pm 1}$ uncertainty in K_{LH}. In the left-hand region we have measured n_{H_2} while $K_{LH}P^{in}_{H_2} \gg K_{LH}P^{in}_{D_2}$ and in the right-hand region we have measured n_{H_2} while $K_{LH}P^{in}_{H_2} \ll K_{LH}P^{in}_{D_2}$ (actually, we have measured n_{D_2} while $K_{LH}P^{in}_{H_2} \gg K_{LH}P^{in}_{D_2}$ but since subsequent discussion is all in terms of n_{H_2} we have

DOI: 10.1021/acscatal.8b02168
ACS Catal. 2018, 8, 10486−10497

represented the right-hand region, which is equivalent to making the measurements of n_{H_2} while $K_{LH}P^{in}_{H_2} \ll K_{LH}P^{in}_{D_2}$).

4.1. Langmuir–Hinshelwood (LH) Mechanism. The LH mechanism depicted at the left of Figure 4 involves the dissociative adsorption and recombinative desorption of H_2, D_2, and HD on the surface with direct competition of H and D for adsorption sites. The steady-state equations describing the coverages of H and D atoms are

$$\frac{d\theta_H}{dt} = 0 = 2k_a^{LH}P_{H_2}(1-\theta)^2 - 2k_d^{LH}\theta_H^2 + k_a^{LH}P_{HD}(1-\theta)^2 - 2k_d^{LH}\theta_H\theta_D \quad (4)$$

$$\frac{d\theta_D}{dt} = 0 = 2k_a^{LH}P_{D_2}(1-\theta)^2 - 2k_d^{LH}\theta_D^2 + k_a^{LH}P_{HD}(1-\theta)^2 - 2k_d^{LH}\theta_D\theta_H \quad (5)$$

where k_a^{LH} and k_d^{LH} are the rate constants for *molecular* adsorption. The factors of 2 in the first two terms of each expression account for the fact that 2 H (D) atoms adsorb and desorb with each molecule of H_2 (D_2). The rate constants are assumed to be identical for both isotopes. Note that the rate for molecular desorption of HD, $2k_d^{LH}\theta_D\theta_H$, is also multiplied by 2 to give the appropriate rates for given coverages θ_H and θ_D. At equilibrium with $P_{H_2} = P_{D_2}$, one has $P_{HD} = 2P_{H_2}$ and the rate of molecular adsorption of HD is twice that of H_2. Therefore, at equilibrium the rate of HD desorption must be $r_{HD}^{des} = 2r_{H_2}^{des} = 2k_d\theta_H\theta_D$, where $\theta_H = \theta_D$. Finally, the total coverage on the surface is given by

$$\theta = \theta_H + \theta_D \quad (6)$$

Under conditions of low H_2–D_2 conversion, $P_{HD} \approx 0$, HD adsorption can be ignored, and the HD formation rate is

$$r_{HD}^{LH} = 2k_d^{LH}\theta_H\theta_D \quad (7)$$

The coverages θ_H and θ_D can be calculated (see Supporting Information section 3) from the steady-state mass balance eqs 4–6 to yield the rate expression

$$r_{HD}^{LH} = \frac{2k_d^{LH}K_{LH}^2P^{in}_{H_2}P^{in}_{D_2}}{(\sqrt{K_{LH}P^{tot}} + K_{LH}P^{tot})^2} \quad (8)$$

The quantity K_{LH} is the equilibrium constant ($K_{LH} = k_a^{LH}/k_d^{LH}$), and $P^{in}_{H_2}$ and $P^{in}_{D_2}$ are the inlet (or initial) partial pressures of H_2 and D_2, respectively.

Extracting the reaction orders from the rate expression uses

$$n_{H_2} = \frac{d\ln r_{HD}}{d\ln P^{in}_{H_2}} \quad (9a)$$

and

$$n_{D_2} = \frac{d\ln r_{HD}}{d\ln P^{in}_{D_2}} \quad (9b)$$

The value of n_{H_2} calculated across ($K_{LH}P^{in}_{H_2}$, $K_{LH}P^{in}_{D_2}$) is shown as a contour plot in Figure 7. In the lower right half of the plot (red region), $K_{LH}P^{in}_{H_2} \ll K_{LH}P^{in}_{D_2}$ and the reaction order is $n_{H_2} = 1$. The value of θ_D is insensitive to θ_H, which is always increasing linearly

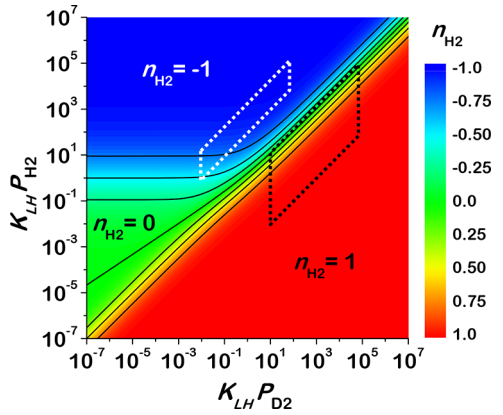

Figure 7. Reaction order in n_{H_2} versus ($K_{LH}P^{in}_{H_2}$,$K_{LH}P^{in}_{D_2}$) for H_2–D_2 exchange via the LH mechanism. The dashed parallelograms demarcate the conditions within which our measurements were conducted.

with $K_{LH}P^{in}_{H_2}$. This is consistent with our observation (Figure 3a) that $n_{D_2} = 0.92$ when $P^{in}_{H_2} \gg P^{in}_{D_2}$. Across the upper left region of Figure 7 where the color is changing from green to blue, $K_{LH}P^{in}_{H_2} \gg K_{LH}P^{in}_{D_2}$. While the total coverage is low, $\theta \cong \sqrt{K_{LH}P^{tot}} \ll 1$, the reaction order is $n_{H_2} = 0$ because increasing $K_{LH}P^{in}_{H_2}$ increases $\theta_H \propto \sqrt{K_{LH}P^{in}_{H_2}}$ but decreases $\theta_D \propto 1/\sqrt{K_{LH}P^{in}_{D_2}}$ proportionately. Once the total coverage becomes high, $\theta_H \approx 1$, the reaction order drops to $n_{H_2} = -1$ because increasing $K_{LH}P^{in}_{H_2}$ cannot increase θ_H further but decreases $\theta_D \propto 1/K_{LH}P^{in}_{H_2}$.

Experimentally, we find that $n_{H_2} \cong 0$ for all Ag_xPd_{1-x} compositions when $K_{LH}P_{H_2} \gg K_{LH}P_{D_2}$ (Figure 3b) and under conditions in which $\theta \approx 1$. However, the classical LH model predicts that $n_{H_2} = -1$ under these conditions. A value of $n_{H_2} \approx 0$ is only expected when $\theta \ll 1$, but this is not consistent with the conditions of our measurements. It has been suggested that subsurface H′ species may participate in the H_2–D_2 exchange mechanism and lead to zero-order kinetics at high coverages, θ.[8,9]

Savara et al. measured the reactions orders for H_2–D_2 exchange on Pd(111) and supported Pd nanoparticles using molecular beam methods.[8] At $T > 280$ K, they observed reaction orders consistent with the classical LH mechanism. However, at $T < 280$ K and $K_{LH}P_{H_2} \ll K_{LH}P_{D_2}$ (in their case), they observe a reaction order of $n_{D_2} \approx 0$, a result that is consistent with ours but not consistent with the predictions of a simple LH model. This transition with temperature is consistent with the conditions under which H′ atoms are present in the subsurface. As such, they hypothesize that subsurface H′ atoms influence the surface reaction mechanism. In the following sections, we analyze three different mechanisms for H_2–D_2 exchange that involve subsurface hydrogen.

4.2. LH Plus Breakthrough (LH+BT) Mechanism. The BT mechanism is illustrated in Figure 4 and involves the adsorption of H_2 depositing one H atom on the surface and the other H′ atom directly into the subsurface. Desorption occurs by a reaction between a subsurface H′ and a surface H to yield gas-phase H_2. The BT mechanism has been proposed and investigated by Savara et al. to explain their values of the reaction orders for H_2–D_2 exchange on Pd(111) and supported Pd nanoparticles.[8] The pure BT model artificially constrains the system to have exactly $\theta_H = \theta'_H$ and $\theta_D = \theta'_D$. We have solved this

DOI: 10.1021/acscatal.8b02168
ACS Catal. 2018, 8, 10486–10497

model in section 5 in the Supporting Information. In this section we describe the more realistic coupled LH+BT model (as was also analyzed by Savara et al.) and its solution (section 7 in the Supporting Information). This model allows $\theta_H \neq \theta'_H$ and $\theta_D \neq \theta'_D$ and, in principle, it describes the transition from conditions in which the LH mechanism dominates the kinetics to conditions under which the BT mechanism dominates.

The solution for the LH+BT model defines total coverage of atoms on the surface and in the subsurface: $\theta = \theta_H + \theta_D$ and $\theta' = \theta'_H + \theta'_D$. The steady-state equations for the four species coverages θ_H, θ'_H, θ_D, and θ'_D are

$$\frac{d\theta_H}{dt} = 0 = 2k_a^{LH}P_{H_2}(1-\theta)^2 - 2k_d^{LH}\theta_H^2 + k_a^{LH}P_{HD}(1-\theta)^2 - 2k_d^{LH}\theta_H\theta_D + k_a^{BT}P_{H_2}(1-\theta)(1-\theta') - k_d^{BT}\theta_H\theta'_H + \frac{1}{2}k_a^{BT}P_{HD}(1-\theta)(1-\theta') - k_d^{BT}\theta_H\theta'_D \quad (10)$$

$$\frac{d\theta'_H}{dt} = 0 = k_a^{BT}P_{H_2}(1-\theta)(1-\theta') - k_d^{BT}\theta'_H\theta_H + \frac{1}{2}k_a^{BT}P_{HD}(1-\theta)(1-\theta') - k_d^{BT}\theta'_H\theta_D \quad (11)$$

$$\frac{d\theta_D}{dt} = 0 = 2k_a^{LH}P_{D_2}(1-\theta)^2 - 2k_d^{LH}\theta_D^2 + k_a^{LH}P_{HD}(1-\theta)^2 - 2k_d^{LH}\theta_D\theta_H + k_a^{BT}P_{D_2}(1-\theta)(1-\theta') - k_d^{BT}\theta_D\theta'_D + \frac{1}{2}k_a^{BT}P_{HD}(1-\theta)(1-\theta') - k_d^{BT}\theta_D\theta'_H \quad (12)$$

$$\frac{d\theta'_D}{dt} = 0 = k_a^{BT}P_{D_2}(1-\theta)(1-\theta') - k_d^{BT}\theta'_D\theta_D + \frac{1}{2}k_a^{BT}P_{HD}(1-\theta)(1-\theta') - k_d^{BT}\theta'_D\theta_H \quad (13)$$

Under conditions of low conversion, $P_{HD} \approx 0$, HD adsorption can be ignored, and the rate of HD formation is

$$r_{HD}^{LH+BT} = 2k_d^{LH}\theta_H\theta_D + k_d^{BT}(\theta_H\theta'_D + \theta'_H\theta_D) \quad (14)$$

The coverages can be calculated from the steady-state mass balance equations 10−13 to yield the rate law

$$r_{HD}^{LH+BT} = \frac{2k_d^{LH}K_{LH}^2P_{H_2}^{in}P_{D_2}^{in}}{(\sqrt{K_{LH}P^{tot}} + K_{LH}P^{tot})^2} + \frac{2k_d^{BT}K_{LH}K_{BT}P_{H_2}^{in}P_{D_2}^{in}}{(\sqrt{K_{LH}P^{tot}} + K_{BT}P^{tot})(\sqrt{K_{LH}P^{tot}} + K_{LH}P^{tot})} \quad (15)$$

The first term is the rate due to the LH mechanism, and the second is due to the BT mechanism. The BT+ssdiff model (see section 6 in the Supporting Information) yields a rate law that is exactly equivalent to the second term in eq 15. Note that both terms have the same functional dependence on pressures. In illustrating the reaction orders, we have eliminated the contributions of the LH term and used only BT+ssdiff term. Inserting the BT+ssdiff term of eq 15 into eq 9a yields the reaction orders n_{H_2} and n_{D_2}. The value of n_{H_2} versus $(K_{LH}P_{H_2}^{in}, K_{LH}P_{D_2}^{in})$ are plotted for $K_{ss} = K_{LH}/K_{BT} = 10^{-4}$ in Figure 8. With $K_{ss} = 10^{-4}$, $K_{LH}P_{H_2}^{in} \gg K_{LH}P_{D_2}^{in}$ and over the range where $\theta_H \approx 1$ but $\theta' \ll 1$, H_2−D_2 exchange has a reaction order of $n_{H_2} = -1/2$. The BT+ssdiff model predicts $n_{H_2} = -1/2$ over the region in which we have measured $n_{H_2} = 0$.

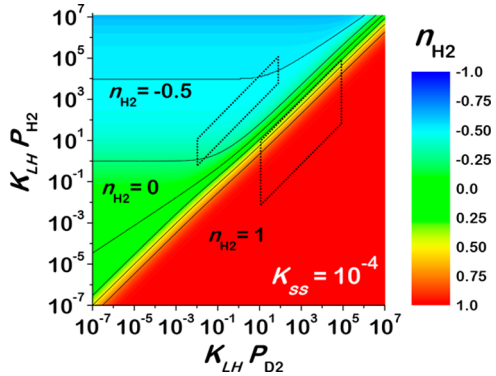

Figure 8. Reaction order n_{H_2} versus $(K_{LH}P_{H_2}^{in}, K_{LH}P_{D_2}^{in})$ for H_2−D_2 exchange via the BT+ssdiff mechanism with $K_{ss} = 10^{-4}$. The dashed parallelograms demarcate the conditions within which our measurements were conducted. These data are shown for $K_{ss} = 10^{-3}$, 10^{-4}, and 10^{-5} in section 10 in the Supporting Information.

4.3. Single Subsurface H′ Plus Surface−Subsurface Diffusion (SH+ssdiff) Mechanism. The third mechanism explored to probe the effect of subsurface H′ or D′ species on the reaction orders for catalytic H_2−D_2 exchange postulates that a single subsurface H′ atom promotes the recombinative desorption of H_2 from the surface sites immediately above it (Figure 4). Similarly, adsorption onto a site with a single subsurface H′ atom must be promoted (Figure 5). Promotion of hydrogen adsorption and desorption means a lowering of the barriers to these two processes relative to those on sites without subsurface H′ atoms (i.e., the LH process; Figure 5). Promotion could also arise from destabilization of the H atoms relative to those on unpromoted sites. The mechanism for H transport into the subsurface to form H′ is modeled as a parallel diffusion process with the equilibrium constant K_{ss}. The details of the combined SH+ssdiff model and its solution are given in section 8 in the Supporting Information.

The steady-state equations describing θ_H, θ'_H, θ_D, and θ'_D are

$$\frac{d\theta_H}{dt} = 0 = 2k_a^{SH}P_{H_2}(1-\theta)^2\theta' - 2k_d^{SH}\theta_H^2\theta' + k_a^{SH}P_{HD}(1-\theta)^2\theta' - 2k_d^{SH}\theta_H\theta_D\theta' - k_{in}^{ss}\theta_H(1-\theta') + k_{out}^{ss}\theta'_H(1-\theta) \quad (16)$$

$$\frac{d\theta'_H}{dt} = 0 = k_{in}^{ss}\theta_H(1-\theta') - k_{out}^{ss}\theta'_H(1-\theta) \quad (17)$$

DOI: 10.1021/acscatal.8b02168
ACS Catal. 2018, 8, 10486−10497

$$\frac{d\theta_D}{dt} = 0 = 2k_a^{SH}P_{D_2}(1-\theta)^2\theta' - 2k_d^{SH}\theta_D^2\theta' + k_a^{SH}P_{HD}(1-\theta)^2\theta' - 2k_d^{SH}\theta_D\theta_H\theta' - k_{in}^{ss}\theta_D(1-\theta') + k_{out}^{ss}\theta_D'(1-\theta) \quad (18)$$

$$\frac{d\theta_D'}{dt} = 0 = k_{in}^{ss}\theta_D(1-\theta') - k_{out}^{ss}\theta_D'(1-\theta) \quad (19)$$

Under conditions of low conversion, $P_{HD} \approx 0$, HD adsorption can be ignored, and the HD formation rate is

$$r_{HD}^{SH+diff} = 2k_d^{SH}\theta_H\theta_D\theta' \quad (20)$$

The coverages can be calculated from the steady-state mass balance equations 16−19 and plugged into eq 20 to give the rate expression

$$r_{HD}^{SH+ssdiff} = \frac{2k_d^{SH}K_{ss}K_{SH}^2P_{H_2}^{in}P_{D_2}^{in}}{\sqrt{K_{SH}P^{tot}}(1+\sqrt{K_{SH}P^{tot}})^2(1+K_{ss}\sqrt{K_{SH}P^{tot}})} \quad (21)$$

where K_{SH} and K_{ss} are the equilibrium constants for adsorption and for surface−subsurface diffusion of H, respectively. Within the context of the Langmuir model for adsorption and valid for low values of θ_H' we have $K_{SH} \approx K_{LH}$. Values of n_{H_2} calculated by inserting eq 21 into eq 9a are plotted versus $(K_{LH}P_{H_2}^{in}, K_{LH}P_{D_2}^{in})$ in Figure 9 for $K_{ss} = 10^{-4}$ (see section 10 in the Supporting Information for plots with K_{ss}= 10^{-3}, 10^{-4}, and 10^{-5}). For $K_{LH}P_{H_2}^{in} \gg K_{LH}P_{D_2}^{in}$ and low coverages, $\theta \ll 1$, the reaction order is $n_{H_2} = 1/2$. For $\theta \approx 1$, the SH-ssdiff model predicts $n_{H_2} = -1/2$ over the region in which we measure $n_{H_2} \approx 0$. Clearly the SH-ssdiff model does not predict our observations.

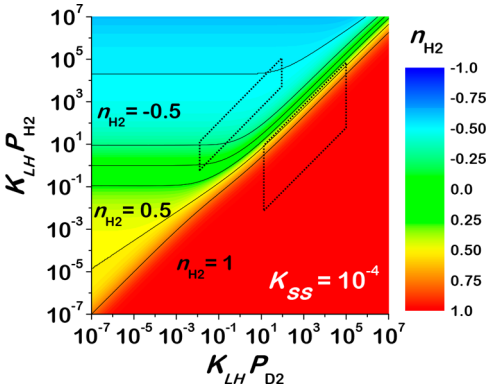

Figure 9. Reaction order in n_{H_2} versus $(K_{LH}P_{H_2}^{in}, K_{LH}P_{D_2}^{in})$ for H_2−D_2 exchange via the SH+ssdiff mechanism with $K_{ss} = 10^{-4}$. The dashed parallelograms demarcate the conditions over which our measurements were conducted. These data are shown for $K_{ss} = 10^{-3}$, 10^{-4} and 10^{-5} in section 10 in the Supporting Information.

4.4. Dual Subsurface Hydrogen Plus Surface−Subsurface Diffusion (DH+ssdiff) Mechanism. The fourth mechanism to capture the effect of the subsurface species and predict the reaction orders for catalytic H_2−D_2 exchange reaction involves the promotion of adjacent H (D) by two adjacent H′ (D′) atoms in the immediate subsurface (Figure 4). This mechanism is coupled with the surface-subsurface diffusion of H(D).

The steady-state equations describing θ_H, θ_H', θ_D, and θ_D' for the DH+ssdiff mechanism are

$$\frac{d\theta_H}{dt} = 0 = 2k_a^{DH}P_{H_2}(1-\theta)^2\theta'^2 - 2k_d^{DH}\theta_H^2\theta'^2 + k_a^{DH}P_{HD}(1-\theta)^2\theta'^2 - 2k_d^{DH}\theta_H\theta_D\theta'^2 - k_{in}^{ss}\theta_H(1-\theta') + k_{out}^{ss}\theta_H'(1-\theta) \quad (22)$$

$$\frac{d\theta_H'}{dt} = 0 = k_{in}^{ss}\theta_H(1-\theta') - k_{out}^{ss}\theta_H'(1-\theta) \quad (23)$$

$$\frac{d\theta_D}{dt} = 0 = 2k_a^{DH}P_{D_2}(1-\theta)^2\theta'^2 - 2k_d^{DH}\theta_D^2\theta'^2 + k_a^{DH}P_{HD}(1-\theta)^2\theta'^2 - 2k_d^{DH}\theta_D\theta_H\theta'^2 - k_{in}^{ss}\theta_D(1-\theta') + k_{out}^{ss}\theta_D'(1-\theta) \quad (24)$$

$$\frac{d\theta_D'}{dt} = 0 = k_{in}^{ss}\theta_D(1-\theta') - k_{out}^{ss}\theta_D'(1-\theta) \quad (25)$$

Under conditions of low conversion, $P_{HD} \approx 0$, HD adsorption can be ignored, and the HD formation rate is

$$r_{HD}^{DH+ssdiff} = 2k_d^{DH}\theta_H\theta_D\theta'^2 \quad (26)$$

The coverages can be calculated from the steady-state mass balance eqs 22−25. These yield the rate law

$$r_{HD}^{DH+ssdiff} = \frac{2k_d^{DH}K_{ss}^2K_{DH}^2P_{H_2}^{in}P_{D_2}^{in}}{(1+\sqrt{K_{DH}P^{tot}})^2(1+K_{SS}\sqrt{K_{DH}P^{tot}})^2} \quad (27)$$

The reaction rate orders with respect to H and D can be calculated by inserting eq 27 into eq 9a. The value of n_{H_2} has been plotted versus $(K_{LH}P_{H_2}^{in}, K_{LH}P_{D_2}^{in})$ in Figure 10 for values of $K_{ss} = 10^{-4}$. The DH+ssdiff mechanism predicts $n_{H_2} = 0$ over the region of $(K_{LH}P_{H_2}^{in}, K_{LH}P_{D_2}^{in})$ in which our measurements were made and are consistent with the result of our measurements.

Having identified the DH+ssdiff mechanism as the one that predicts $n_{H_2} = 0$ for $K_{LH}P_{H_2}^{in} \gg K_{LH}P_{D_2}^{in}$, we can examine eq 26 to understand the origin of our observed reaction order. By examining the coverages as shown in Figure 6 and their expressions found in Table 1, it is clear that $\theta_H \approx 1$ under the measurement conditions and will be insensitive to increases in $P_{H_2}^{in}$. On the other hand, $\theta_D \approx 0$ and scales proportionately to $(P_{H_2}^{in})^{-1}$, as expected in the LH mechanism. The key point is that $\theta_D \propto (P_{H_2}^{in})^{-1}$ is compensated for by the subsurface coverage, $\theta' \approx 0$. The value of θ'^2 scales $\propto P_{H_2}^{in}$. Thus, in eq 26 we have the terms $\theta_H\theta_D\theta'^2 \propto (P_{H_2}^{in})^0$ and the prediction of n_{H_2}= 0 for $K_{LH}P_{H_2}^{in} \gg K_{LH}P_{D_2}^{in}$. It is important to note that for extremely high values of $K_{LH}P_{H_2}^{in}$ that are off scale on Figure 10, the subsurface layer becomes saturated, $\theta' \approx 1$, and $\theta'^2 \propto (P_{H_2}^{in})^0$ resulting in $\theta_H\theta_D\theta'^2 \propto (P_{H_2}^{in})^{-1}$: i.e., the recurrence of $n_{H_2} = -1$ as in the LH mechanism.

4.5. Summary of H_2−D_2 Exchange Kinetics Involving Subsurface Hydrogen. The adsorption isotherm expressions for the total coverages θ and θ' as functions of P^{tot} derived from

DOI: 10.1021/acscatal.8b02168
ACS Catal. 2018, 8, 10486−10497

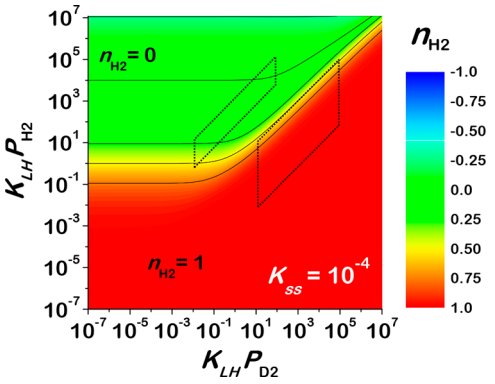

Figure 10. Reaction order in n_{H_2} versus $(K_{LH}P^{in}_{H_2}, K_{LH}P^{in}_{D_2})$ for H_2-D_2 exchange via the DH+ssdiff mechanism with $K_{ss} = 10^{-4}$. The dashed tetragons demarcate the conditions within which our measurements were conducted. These data are shown for $K_{ss} = 10^{-3}$, 10^{-4} and 10^{-5} in section 10 in the Supporting Information.

the four H_2-D_2 exchange mechanisms and their combination with a surface−subsurface diffusion process are all given in Table 1.

Table 1. Summary of the Calculated Surface and Subsurface Coverages Using the Seven Different H_2-D_2 Exchange Mechanisms Proposed[a]

mech	θ[b]	θ'[b]
LH[c]	$\frac{K_{LH}P^{tot}}{\sqrt{K_{LH}P^{tot}} + K_{LH}P^{tot}}$	0
LH+ssdiff	$\frac{K_{LH}P^{tot}}{\sqrt{K_{LH}P^{tot}} + K_{LH}P^{tot}}$	$\frac{K_{ss}K_{LH}P^{tot}}{\sqrt{K_{ss}K_{LH}P^{tot}} + K_{ss}K_{LH}P^{tot}}$
BT[d]	$\frac{K_{BT}P^{tot}}{\sqrt{K_{LH}P^{tot}} + K_{BT}P^{tot}}$	$\frac{K_{BT}P^{tot}}{\sqrt{K_{LH}P^{tot}} + K_{BT}P^{tot}}$
BT+ssdiff	$\frac{\frac{K_{BT}}{K_{ss}}P^{tot}}{\sqrt{\frac{K_{BT}}{K_{ss}}P^{tot}} + \frac{K_{BT}}{K_{ss}}P^{tot}}$	$\frac{K_{ss}K_{BT}P^{tot}}{\sqrt{K_{ss}K_{BT}P^{tot}} + K_{ss}K_{BT}P^{tot}}$
BT+LH	$\frac{K_{LH}P^{tot}}{\sqrt{K_{LH}P^{tot}} + K_{LH}P^{tot}}$	$\frac{K_{BT}P^{tot}}{\sqrt{K_{LH}P^{tot}} + K_{BT}P^{tot}}$
SH+ssdiff	$\frac{K_{SH}P^{tot}}{\sqrt{K_{SH}P^{tot}} + K_{SH}P^{tot}}$	$\frac{K_{ss}K_{SH}P^{tot}}{\sqrt{K_{ss}K_{DH}P^{tot}} + K_{ss}K_{DH}P^{tot}}$
DH+ssdiff	$\frac{K_{DH}P^{tot}}{\sqrt{K_{DH}P^{tot}} + K_{DH}P^{tot}}$	$\frac{K_{ss}K_{DH}P^{tot}}{\sqrt{K_{ss}K_{DH}P^{tot}} + K_{ss}K_{DH}P^{tot}}$
common form[b]	$\frac{K_{LH}P^{tot}}{\sqrt{K_{LH}P^{tot}} + K_{LH}P^{tot}}$	$\frac{K_{ss}K_{LH}P^{tot}}{\sqrt{K_{ss}K_{LH}P^{tot}} + K_{ss}K_{LH}P^{tot}}$

[a]The step-by-step calculations for all these models can be found in the Supporting Information. The coverages of the individual species are given by $\theta_H = \theta P^{in}_{H2}/P^{tot}$ and equivalent expressions for θ_D, θ'_H, and θ'_D. [b]Note that the isotherms for both the surface species, θ, and the subsurface species, θ', are identical for all reaction mechanisms given the relation among the equilibrium constants: $K_{BT} = K_{ss}K_{LH}$. The common form of the last row assumes $K_{SH} = K_{DH} = K_{LH}$. [c]The LH mechanism represents a special case in which $K_{ss} = 0$. [d]The BT mechanism represents a special case in which $K_{ss} = 1$.

It is important to note that in a batch reactor these hold for all extents of reaction because the total hydrogen pressure, $P^{tot} = P^{in}_{H_2} + P^{in}_{D_2}$, whether in the form of H_2, HD, or D_2 is constant. In a flow reactor, the expression in Table 1 holds along the length of the reactor independent of the degree of conversion of H_2 and D_2 conversion to HD. The expressions in Table 1 are parametrized by the equilibrium constants for the five processes defined in Figure 4 and by the potential energy diagram in Figure 5: K_{LH}, K_{BT}, K_{SH}, K_{DH}, and K_{ss}. It is important to appreciate that all of these expressions describe the same equilibrium and that they are all equivalent to one another. The common forms are given in the bottom row of Table 1. These hold because $K_{BT} = K_{ss}K_{LH}$. In the cases of the SH and DH mechanisms, the basic Langmuir assumption that species are noninteracting gives $K_{LH} = K_{SH} = K_{DH}$, which is a good assumption for low values of θ' (consistent with the conditions of our measurements). The LH mechanism can be considered the special case of the subsurface hydrogen mechanism in which $K_{ss} = 0$ and $\theta' = 0$. Likewise, the pure BT mechanism is the special case in which $K_{ss} = 1$ and $\theta' = \theta$. The fact that all coverage expressions in Table 1 are equivalent should not be surprising, given that these equilibria must be path independent.

The rate laws for the different H_2-D_2 exchange mechanisms, in the limit of low conversion, are given in Table 2 in terms of the rate constants for hydrogen desorption, k_d, and in terms of the equilibrium constants K_{LH} and K_{ss}. In the case of the pure BT mechanism, $K_{ss} = 1$. The rate constants for hydrogen desorption are mechanism specific. In all of the rate expressions, the numerator is proportional to $P^{in}_{H_2}P^{in}_{D_2}$. The denominators are parametrized in terms of K_{ss} and $K_{LH}P^{tot}$, where $P^{tot} \approx P^{in}_{H_2} \gg P^{in}_{D_2}$ under the conditions of our experiments.

The fingerprints of subsurface H′ in the kinetics of the H_2-D_2 exchange mechanism arise purely from the terms in the denominators of the rates laws. The rate laws for the LH and LH+ssdiff mechanisms are identical because the presence of H′ has no influence on the surface reactions. Similarly, the LH and pure BT mechanisms have the same rate dependence because the pure BT mechanism enforces $K_{ss} = 1$ and $\theta = \theta'$. Effectively, $K_{BT} = K_{LH}$ for the purely BT mechanism. Note that the LH+BT mechanism yields a rate law with two terms, one equivalent to the LH mechanism and the other equivalent to the BT+ssdiff mechanism. Although surface−subsurface diffusion has not been explicitly considered in the LH+BT mechanism, the inclusion of the LH mechanism provides a pathway for redistribution of H and H′, allowing the surface and subsurface coverages to equilibrate. As can be seen from the coverage expressions in Table 1 and the rate laws in Table 2, they establish the same equilibrium as reached by the BT+ssdiff process; i.e., the equilibrium is path independent. These observations verify that the analysis of the various mechanisms considered in this work has been self-consistent.

Finally, the "fingerprints" of the various subsurface mechanisms evaluated herein are summarized in Table 3. The first two rows establish the four regimes of P^{tot} that yield the various possible values of n_{H_2} while the third and fourth rows give the regimes of adsorbate coverage, θ and θ' corresponding to those operating conditions. The final four rows give the various value of n_{H_2} under conditions of $K_{LH}P^{in}_{H_2} \gg K_{LH}P^{in}_{D_2}$ that one might expect to observe for the four reaction mechanisms compared in this work. In essence this summarizes the findings of Figures 7−10. For conditions of $K_{LH}P^{in}_{H_2} \ll K_{LH}P^{in}_{D_2}$, one always has $n_{H_2} = 1$. For extremely high pressures at which both the surface and the subsurface are saturated with hydrogen, all four mechanisms predict that $n_{H_2} = -1$. At intermediate conditions one can saturate the surface but not the subsurface resulting in pressure

DOI: 10.1021/acscatal.8b02168
ACS Catal. 2018, 8, 10486−10497

Table 2. Rate Laws for the Seven Different H_2-D_2 Exchange Mechanisms Defined Using $K_{BT} = K_{ss}K_{LH}$ and $K_{SH} = K_{DH} = K_{LH}$[a]

mech	r_{HD}	rate law
LH	$2k_d^{LH}\theta_H\theta_D$	$\frac{2k_d^{LH}K_{LH}^2P_{H_2}^{in}}{\left(\sqrt{K_{LH}P^{tot}} + K_{LH}P^{tot}\right)^2}$
LH+ssdiff	$2k_d^{LH}\theta_H\theta_D$	$\frac{2k_d^{LH}K_{LH}^2P_{H_2}^{in}}{\left(\sqrt{K_{LH}P^{tot}} + K_{LH}P^{tot}\right)^2}$
BT	$k_d^{BT}(\theta_H\theta_D' + \theta'\theta_D)$	$\frac{2k_d^{BT}K_{LH}^2P_{H_2}^{in}}{\left(\sqrt{K_{LH}P^{tot}} + K_{LH}P^{tot}\right)^2}$
BT+ssdiff	$k_d^{BT}(\theta_H\theta_D' + \theta_D\theta_H')$	$\frac{2k_d^{LH}k_{LH}^2P_{H_2}^{in}P_{D_2}^{in}}{\left(\sqrt{K_{LH}P^{tot}} + K_{LH}P^{tot}\right)\left(\sqrt{K_{LH}P^{tot}} + K_{ss}K_{LH}P^{tot}\right)}$
LH+BT	$2k_d^{LH}\theta_H\theta_D + k_d^{BT}(\theta_H\theta_D' + \theta_H'\theta_D)$	$\frac{2k_d^{LH}k_{LH}^2P_{H_2}^{in}P_{D_2}^{in}}{\left(\sqrt{K_{LH}P^{tot}} + K_{LH}P^{tot}\right)^2} + \frac{2k_d^{BT}K_{ss}K_{LH}^2P_{H_2}^{in}P_{D_2}^{in}}{\left(\sqrt{K_{LH}P^{tot}} + K_{LH}P^{tot}\right)\left(\sqrt{K_{LH}P^{tot}} + K_{ss}K_{LH}P^{tot}\right)}$
SH+ssdiff	$2k_d^{SH}\theta_H\theta_D\theta'$	$\frac{2k_d^{SH}K_{ss}K_{LH}^2P_{H_2}^{in}P_{D_2}^{in}}{\left(1 + \sqrt{K_{LH}P^{tot}}\right)^2\left(\sqrt{K_{LH}P^{tot}} + K_{ss}K_{LH}P^{tot}\right)}$
DH+ssdiff	$2k_d^{DH}\theta_H\theta_D\theta'^2$	$\frac{2k_d^{DH}K_{ss}^2K_{LH}^2P_{H_2}^{in}P_{D_2}^{in}}{\left(1 + \sqrt{K_{LH}P^{tot}}\right)^2\left(1 + K_{ss}\sqrt{K_{LH}P^{tot}}\right)^2}$

[a]The derivation of each rate law and their explicit forms unconstrained by the previous equalities can be found in the Supporting Information.

Table 3. Reaction Orders n_{H_2} for $P_{H_2}^{in} \gg P_{D_2}^{in}$, Predicted for H_2-D_2 Exchange Mechanisms under Various Reaction Conditions[a]

	Reaction Conditions			
$\sqrt{K_{LH}P^{tot}}$	$\gg 1$	$\gg 1$	$\ll 1$	$\ll 1$
$K_{ss}\sqrt{K_{LH}P^{tot}}$	$\gg 1$	$\ll 1$	$\gg 1$	$\ll 1$
	Coverages			
θ	$\cong 1$	$\cong 1$	$\cong 0$	$\cong 0$
θ'	$\cong 1$	$\cong 0$	$\cong 1$	$\cong 0$
	Reaction Order in $P_{H_2}^{in}$			
$n_{H_2}^{LH}$	-1	n/a	n/a	0
$n_{H_2}^{BT+ssdiff}$	-1	$-1/2$	$-1/2$	0
$n_{H_2}^{SH+ssdiff}$	-1	$-1/2$	0	1/2
$n_{H_2}^{DH+ssdiff}$	-1	0	0	1

[a]The experimental conditions are consistent with $\theta \cong 1$ and $\theta' \cong 0$. The measured value of $n_{H_2} = 0.01$ is consistent with the predicted value of $n_{H_2}^{DH}$.

regimes over which one can observe $n_{H_2} = -1/2$ for the BT +ssdiff and for the SH+ssdiff mechanisms. Note that conditions consistent with the third column in which $K_{ss} > 1$ seem unlikely to exist, since they imply that H′ in the subsurface is energetically stable relative to H on the surface.[27] This would yield regimes in which the subsurface was saturated but the surface was not. Finally, at very low pressures at which neither the surface nor the subsurface are saturated, the various mechanisms exhibit $n_{H_2} = 0$ (BT+ssdiff), 1/2 (SH+ssdiff), and 1 (DH+ssdiff). Of these scenarios, it is clear that the DH+ssdiff model is the only one consistent with our observations of $n_{H_2} = 0$ under conditions which yield a saturated surface and a low concentration of H′ in the subsurface.

4.6. Relaxation of the Assumption That $K_{LH} = K_{SH} = K_{DH}$.

The analysis performed above indicates that, among the mechanisms considered for H_2-D_2 exchange on the Ag_xPd_{1-x} alloys, the DH+ssdiff mechanism is the only one capable of predicting the reaction order $n_{H_2} = 0$ for $K_{LH}P_{H_2}^{in} \gg K_{LH}P_{D_2}^{in}$ and $\theta \approx 1$. It is important to note that, as with all such analyses, this work merely identifies the most likely mechanism among those considered. There must be others that would predict the observed reaction orders. Our analysis above has adhered strictly to the Langmuir assumption that adsorbed species are non-interacting, the simplest possible model. The only interactions are in the transition states to adsorption and desorption (Figure 5), whose energies are influence by subsurface H′ atoms. We have not considered the impact of coverage-dependent adsorption energetics. The justification for ignoring the possible coverage dependence of adsorption energetics is that over the range of conditions of our measurements of n_{H_2} there is very little coverage variation. The values of $\theta \approx 1$ and $\theta' \approx 0$ (Figure 6) over the range of conditions under which we have observed $n_{H_2} = 0$.

Strict adherence to the Langmuir model for adsorption mandates that $K_{LH} = K_{SH} = K_{DH}$ (Figure 5) in that there should be no influence of H′ on the energetics of H other than to influence kinetic barriers to H adsorption and desorption. Relaxing the assumption that $K_{LH} = K_{SH} = K_{DH}$ does not affect the predictions regarding reaction order. To rationalize this, we will refer to H (or D) atoms adsorbed at promoted sites on the surface (with either H′ or D′ in the immediate subsurface) as H* (or D*). If $K_{LH} = K_{SH} = K_{DH}$, the fractional coverage on the

DOI: 10.1021/acscatal.8b02168
ACS Catal. 2018, 8, 10486−10497

promoted site will be identical with that on the unprompted sites, $\theta = \theta^*$, because the adsorption energetics are identical on both sites. If the adsorption energetics on the promoted and unpromoted sites are different,[57] $K_{LH} \neq K_{SH} \neq K_{DH}$, and $\theta \neq \theta^*$. Under steady-state reaction conditions with $\theta \approx 1$, the reaction is desorption rate limited and the coverages on the surface are in pseudoequilibrium with the gas phase, as indicated in Table 1. The subsurface coverages θ', θ'_H, and θ'_D are equilibrated with the surface coverages θ, θ_H and θ_D via the surface−subsurface equilibrium constant K_{ss}. In the same way, the coverages on the promoted sites θ^*, θ^*_H, and θ^*_D would be equilibrated with the surface coverages θ, θ_H, and θ_D via an equilibrium constant K^*. The solutions for the coverages θ^*_H and θ^*_D on the prompted sites have the same form as the solutions for θ'_H and θ'_D in the subsurface.

$$\theta^*_H = \frac{K^* K_{LH} P^{tot}}{\sqrt{K_{LH} P^{tot}} + K^* K_{LH} P^{tot}} \left(\frac{P^{in}_{H_2}}{P^{tot}} \right) \tag{28}$$

and

$$\theta^*_D = \frac{K^* K_{LH} P^{tot}}{\sqrt{K_{LH} P^{tot}} + K^* K_{LH} P^{tot}} \left(\frac{P^{in}_{D_2}}{P^{tot}} \right) \tag{29}$$

The reaction orders for the H_2−D_2 exchange are dictated simply by the pressure dependence of the coverages. In the case of the DH+ssdiff mechanism, where the reaction occurs on the promoted sites, the rate is $\propto \theta^*_H \theta^*_D \theta'^2$. The promoted surface sites are saturated, $\theta^* \approx 1$, when $K^* \sqrt{K_{LH} P^{tot}} \gg 1$. Under these conditions and with $P^{in}_{H_2} \gg P^{in}_{D_2}$ we have $\theta^*_H \propto (P^{in}_{H_2})^0$, $\theta^*_D \propto (P^{in}_{H_2})^{-1}$ and $\theta'^2 \propto (P^{in}_{H_2})^1$, leading to a net reaction order in $P^{in}_{H_2}$ of $n_{H_2} = 0$. Following the same reasoning, the reaction orders predicted for the other mechanisms analyzed using the assumption that $K_{LH} = K_{SH} = K_{DH}$ will not change by relaxation of that assumption, provided that the presence of subsurface H′ does not energetically destabilize adsorbed H to the point that the coverage on the promoted sites becomes $\theta^* \ll 1$.

5. CONCLUSIONS

The Langmuir−Hinshelwood (LH), breakthrough (BT), single-subsurface H′ activation (SH), and dual-subsurface H′ activation (DH) mechanisms for H_2−D_2 exchange, coupled with surface−subsurface diffusion (ssdiff) of H and D, have been shown to have kinetically distinguishable rate laws. These exhibit reaction orders, n_{H_2} for $P^{in}_{H_2} \gg P^{in}_{D_2}$, across the range of possible reaction conditions that have values characterstic of each mechanism. This makes possible the experimental identification of the subsurface hydrogen mechanism active for H_2−D_2 exchange. Our measurements on Ag_xPd_{1-x} alloys with $x = 0$−0.9 and previously published results on the Pd(111) surface and on Pd nanoparticles reveal that $n_{H_2} = 0$ for $P^{in}_{H_2} \gg P^{in}_{D_2}$. This is consistent with the dual-subsurface H′ (D′) activation mechanism (DH+ssdiff), in which two adjacent subsurface H′ or D′ atoms activate the recombinative desorption of adjacent pairs of H (D) atoms on the surface.

■ ASSOCIATED CONTENT

Supporting Information

The Supporting Information is available free of charge on the ACS Publications website at DOI: 10.1021/acscatal.8b02168.

Conditions under which H_2−D_2 exchange kinetics have been measured on Ag_xPd_{1-x} alloys, graphical representation of all of the kinetic data, detailed analyses of the steady-state kinetic equations describing the various mechanistic models considered in this study, and graphical representations of the reaction orders predicted for all four models for a range of values of the surface−subsurface H atom diffusion constant, K_{ss} (PDF)

■ AUTHOR INFORMATION

Corresponding Author

*A.J.G.: tel, (412) 268-3848; e-mail, gellman@cmu.edu.

ORCID

Andrew J. Gellman: 0000-0001-6618-7427

Notes

The authors declare no competing financial interest.

■ ACKNOWLEDGMENTS

This work has been funded by the US NSF under grant number NSF-CHE1566228. We thank A. Savara for discussions of the BT mechanism.

■ REFERENCES

(1) van den Berg, A. W. C.; Arean, C. O. Materials for Hydrogen Storage: Current Research Trends and Perspectives. *Chem. Commun.* **2008**, *6*, 668−681.

(2) Raimondi, F.; Scherer, G. G.; Kötz, R.; Wokaun, A. Nanoparticles in Energy Technology: Examples from Electrochemistry and Catalysis. *Angew. Chem., Int. Ed.* **2005**, *44*, 2190−2209.

(3) Satterfield, C. N. *Heterogeneous Catalysis in Industrial Practice*; McGraw Hill: New York, 1991; p 542.

(4) Chorkendorff, I.; Niemantsverdriet, J. *Concepts of Modern Catalysis and Kinetics*, 3rd ed.; Wiley: New York, 2017; p 524.

(5) Somorjai, G. A.; Li, Y. *Introduction to Surface Chemistry and Catalysis*, 2nd ed.; Wiley: New York, 2010; p 771.

(6) Lisowski, W. Kinetics of Hydrogen Adsorption and Desorption on Thin Platinum Films. *Appl. Surf. Sci.* **1988**, *31*, 451−459.

(7) Christmann, K. Interaction of Hydrogen with Solid Surfaces. *Surf. Sci. Rep.* **1988**, *9*, 1−163.

(8) Savara, A.; Ludwig, W.; Schauermann, S. Kinetic Evidence for a Non-Langmuir-Hinshelwood Surface Reaction: H/D Exchange over Pd Nanoparticles and Pd(111). *ChemPhysChem* **2013**, *14*, 1686−1695.

(9) Ludwig, W.; Savara, A.; Madix, R. J.; Schauermann, S.; Freund, H.-J. Subsurface Hydrogen Diffusion into Pd Nanoparticles: Role of Low-Coordinated Surface Sites and Facilitation by Carbon. *J. Phys. Chem. C* **2012**, *116*, 3539−3544.

(10) Daley, S. P.; Utz, A. L.; Trautman, T. R.; Ceyer, S. T. Ethylene Hydrogenation on Ni(111) by Bulk Hydrogen. *J. Am. Chem. Soc.* **1994**, *116*, 6001−6002.

(11) Doyle, A. M.; Shaikhutdinov, S. K.; Jackson, S. D.; Freund, H. J. Hydrogenation on Metal Surfaces: Why Are Nanoparticles More Active Than Single Crystals? *Angew. Chem., Int. Ed.* **2003**, *42*, 5240−5243.

(12) Teschner, D.; Borsodi, J.; Wootsch, A.; Révay, Z.; Hävecker, M.; Knop-Gericke, A.; Jackson, S. D.; Schlögl, R. The Roles of Subsurface Carbon and Hydrogen in Palladium-Catalyzed Alkyne Hydrogenation. *Science* **2008**, *320*, 86−89.

(13) Stacchiola, D.; Tysoe, W. T. The Effect of Subsurface Hydrogen on the Adsorption of Ethylene on Pd(111). *Surf. Sci.* **2003**, *540*, L600−L604.

(14) Johnson, A. D.; Daley, S. P.; Utz, A. L.; Ceyer, S. T. The Chemistry of Bulk Hydrogen: Reaction of Hydrogen Embedded in Nickel with Adsorbed CH_3. *Science* **1992**, *257*, 223−225.

(15) Johnson, A. D.; Maynard, K. J.; Daley, S. P.; Yang, Q. Y.; Ceyer, S. T. Hydrogen Embedded in Ni: Production by Incident Atomic Hydrogen and Detection by High-Resolution Electron Energy Loss. *Phys. Rev. Lett.* **1991**, *67*, 927−930.

(16) Maynard, K. J.; Johnson, A. D.; Daley, S. P.; Ceyer, S. T. A New Mechanism for Absorption: Collision-Induced Absorption. *Faraday Discuss. Chem. Soc.* **1991**, *91*, 437−449.

DOI: 10.1021/acscatal.8b02168
ACS Catal. 2018, 8, 10486−10497

(17) Wilde, M.; Fukutani, K.; Ludwig, W.; Brandt, B.; Fischer, J. H.; Schauermann, S.; Freund, H. J. Influence of Carbon Deposition on the Hydrogen Distribution in Pd Nanoparticles and Their Reactivity in Olefin Hydrogenation. *Angew. Chem., Int. Ed.* **2008**, *47*, 9289−9293.
(18) Wilde, M.; Fukutani, K.; Naschitzki, M.; Freund, H. J. Hydrogen Absorption in Oxide-Supported Palladium Nanocrystals. *Phys. Rev. B: Condens. Matter Mater. Phys.* **2008**, *77*, 113412.
(19) Zhang, Q.; Li, J.; Liu, X.; Zhu, Q. Synergetic Effect of Pd and Ag Dispersed on Al_2O_3 in the Selective Hydrogenation of Acetylene. *Appl. Catal., A* **2000**, *197*, 221−228.
(20) Khan, N. A.; Shaikhutdinov, S.; Freund, H.-J. Acetylene and Ethylene Hydrogenation on Alumina Supported Pd-Ag Model Catalysts. *Catal. Lett.* **2006**, *108*, 159−164.
(21) Studt, F.; Abild-Pedersen, F.; Bligaard, T.; Sorensen, R. Z.; Christensen, C. H.; Norskov, J. K. Identification of Non-Precious Metal Alloy Catalysts for Selective Hydrogenation of Acetylene. *Science* **2008**, *320*, 1320−1322.
(22) Adams, B. D.; Chen, A. The Role of Palladium in a Hydrogen Economy. *Mater. Today* **2011**, *14*, 282−289.
(23) Amandusson, H.; Ekedahl, L.-G.; Dannetun, H. Hydrogen Permeation through Surface Modified Pd and PdAg Membranes. *J. Membr. Sci.* **2001**, *193*, 35−47.
(24) Jayaraman, V.; Lin, Y. S. Synthesis and Hydrogen Permeation Properties of Ultrathin Palladium-Silver Alloy Membranes. *J. Membr. Sci.* **1995**, *104*, 251−262.
(25) Shu, J.; Grandjean, B. P. A.; Neste, A. V.; Kaliaguine, S. Catalytic Palladium-Based Membrane Reactors: A Review. *Can. J. Chem. Eng.* **1991**, *69*, 1036−1060.
(26) Conrad, H.; Ertl, G.; Latta, E. E. Adsorption of Hydrogen on Palladium Single Crystal Surfaces. *Surf. Sci.* **1974**, *41*, 435−446.
(27) Ferrin, P.; Kandoi, S.; Nilekar, A. U.; Mavrikakis, M. Hydrogen Adsorption, Absorption and Diffusion on and in Transition Metal Surfaces: A DFT Study. *Surf. Sci.* **2012**, *606*, 679−689.
(28) Herron, J. A.; Tonelli, S.; Mavrikakis, M. Atomic and Molecular Adsorption on Pd(111). *Surf. Sci.* **2012**, *606*, 1670−1679.
(29) Felter, T. E.; Stulen, R. H.; Koszykowski, M. L.; Gdowski, G. E.; Garrett, B. Experimental and Theoretical Investigation of Hydrogen Diffusion on a Metal Surface. *J. Vac. Sci. Technol., A* **1989**, *7*, 104−107.
(30) Gdowski, G. E.; Felter, T. E.; Stulen, R. H. Effect of Surface Temperature on the Sorption of Hydrogen by Pd(111). *Surf. Sci.* **1987**, *181*, L147−L155.
(31) Michalak, W. D.; Miller, J. B.; Alfonso, D. R.; Gellman, A. J. Uptake, Transport, and Release of Hydrogen from Pd(100). *Surf. Sci.* **2012**, *606*, 146−155.
(32) Eichler, A.; Hafner, J.; Groß, A.; Scheffler, M. Trends in the Chemical Reactivity of Surfaces Studied by Ab Initio Quantum-Dynamics Calculations. *Phys. Rev. B: Condens. Matter Mater. Phys.* **1999**, *59*, 13297−13300.
(33) Eichler, A.; Kresse, G.; Hafner, J. Ab-Initio Calculations of the 6d Potential Energy Surfaces for the Dissociative Adsorption of H_2 on the (100) Surfaces of Rh, Pd and Ag. *Surf. Sci.* **1998**, *397*, 116−136.
(34) Montoya, A.; Schlunke, A.; Haynes, B. S. Reaction of Hydrogen with Ag(111): Binding States, Minimum Energy Paths, and Kinetics. *J. Phys. Chem. B* **2006**, *110*, 17145−17154.
(35) Greeley, J.; Mavrikakis, M. Surface and Subsurface Hydrogen: Adsorption Properties on Transition Metals and near-Surface Alloys. *J. Phys. Chem. B* **2005**, *109*, 3460−3471.
(36) Knapton, A. G. Palladium Alloys for Hydrogen Diffusion Membranes. *Platinum Met. Rev.* **1977**, *21*, 44−50.
(37) Versuchen, N.; Jurisch, E.; Metz, A. The Solubility of Hydrogen in Solid Alloys of Palladium with Gold, Silver and Platinum. *Z. Anorg. Allg. Chem.* **1915**, *92*, 329−362.
(38) Sieverts, A.; Hagen, H. The Electrical Resistence of Hydrogen Rotations from Alloys of Palladium with Silver and Gold. *Z. Phys. Chem. A-Chem. Thermodyn. Kinet. Elektrochem. Eigensch.lehre* **1935**, *174*, 247−261.
(39) Mei, D.; Neurock, M.; Smith, C. M. Hydrogenation of Acetylene−Ethylene Mixtures over Pd and Pd−Ag Alloys: First-Principles-Based Kinetic Monte Carlo Simulations. *J. Catal.* **2009**, *268*, 181−195.
(40) Studt, F.; Abild-Pedersen, F.; Bligaard, T.; Sørensen, R. Z.; Christensen, C. H.; Nørskov, J. K. On the Role of Surface Modifications of Palladium Catalysts in the Selective Hydrogenation of Acetylene. *Angew. Chem., Int. Ed.* **2008**, *47*, 9299−9302.
(41) Wilde, M.; Ohno, S.; Ogura, S.; Fukutani, K.; Matsuzaki, H. Quantification of Hydrogen Concentrations in Surface and Interface Layers and Bulk Materials through Depth Profiling with Nuclear Reaction Analysis. *J. Visualized Exp.* **2016**, *109*, e53452.
(42) Yang, B.; Burch, R.; Hardacre, C.; Headdock, G.; Hu, P. Influence of Surface Structures, Subsurface Carbon and Hydrogen, and Surface Alloying on the Activity and Selectivity of Acetylene Hydrogenation on Pd Surfaces: A Density Functional Theory Study. *J. Catal.* **2013**, *305*, 264−276.
(43) Fleutot, B.; Miller, J. B.; Gellman, A. J. Apparatus for Deposition of Composition Spread Alloy Films: The Rotatable Shadow Mask. *J. Vac. Sci. Technol., A* **2012**, *30*, 061511.
(44) Wei, T.; Wang, J.; Goodman, D. W. Characterization and Chemical Properties of Pd−Au Alloy Surfaces. *J. Phys. Chem. C* **2007**, *111*, 8781−8788.
(45) Priyadarshini, D.; Kondratyuk, P.; Picard, Y. N.; Morreale, B. D.; Gellman, A. J.; Miller, J. B. High-Throughput Characterization of Surface Segregation in Cu_xPd_{1-x} Alloys. *J. Phys. Chem. C* **2011**, *115*, 10155−10163.
(46) He, J. W.; Shea, W. L.; Jiang, X.; Goodman, D. W. Surface Chemistry of Monolayer Metallic Films on Re(0001) and Mo(110). *J. Vac. Sci. Technol., A* **1990**, *8*, 2435−2444.
(47) Park, C.; Bauer, E.; Poppa, H. Growth and Alloying of Pd Films on Mo(110) Surfaces. *Surf. Sci.* **1985**, *154*, 371−393.
(48) Boes, J. R.; Kondratyuk, P.; Yin, C. R.; Miller, J. B.; Gellman, A. J.; Kitchin, J. R. Core Level Shifts in Cu-Pd Alloys as a Function of Bulk Composition and Structure. *Surf. Sci.* **2015**, *640*, 127−132.
(49) Kondratyuk, P.; Gumuslu, G.; Shukla, S.; Miller, J. B.; Morreale, B. D.; Gellman, A. J. A Microreactor Array for Spatially Resolved Measurement of Catalytic Activity for High-Throughput Catalysis Science. *J. Catal.* **2013**, *300*, 55−62.
(50) McQuarrie, D. A. *Statistical Mechanics*; University Science Books: Mill Valley, CA 2000; p 640.
(51) Yin, C.; Miller, J. B.; Kondratyuk, P.; Gellman, A. J. Detection of CuAuPd Phase Boundaries Using Core Level Shifts. *J. Phys. Chem. B* **2018**, *122*, 764−769.
(52) O'Brien, C. P.; Miller, J. B.; Morreale, B. D.; Gellman, A. J. The Kinetics of H_2−D_2 Exchange over Pd, Cu, and PdCu Surfaces. *J. Phys. Chem. C* **2011**, *115*, 24221−24230.
(53) Dumesic, J. A. *The Microkinetics of Heterogeneous Catalysis*; American Chemical Society: Washington, DC, 1993; p 315.
(54) Johansson, M.; Skúlason, E.; Nielsen, G.; Murphy, S.; Nielsen, R. M.; Chorkendorff, I. Hydrogen Adsorption on Palladium and Palladium Hydride at 1 bar. *Surf. Sci.* **2010**, *604*, 718−729.
(55) Watson, G. W.; Wells, R. P. K.; Willock, D. J.; Hutchings, G. J. A Comparison of the Adsorption and Diffusion of Hydrogen on the {111} Surfaces of Ni, Pd, and Pt from Density Functional Theory Calculations. *J. Phys. Chem. B* **2001**, *105*, 4889−4894.
(56) Dong, W.; Ledentu, V.; Sautet, P.; Eichler, A.; Hafner, J. Hydrogen Adsorption on Palladium: A Comparative Theoretical Study of Different Surfaces. *Surf. Sci.* **1998**, *411*, 123−136.
(57) Aleksandrov, H. A.; Vines, F.; Ludwig, W.; Schauermann, S.; Neyman, K. M. Tuning the Surface Chemistry of Pd by Atomic C and H: A Microscopic Picture. *Chem. - Eur. J.* **2013**, *19*, 1335−1345.
(58) Boes, J. R.; Gumuslu, G.; Miller, J. B.; Gellman, A. J.; Kitchin, J. R. Estimating Bulk-Composition-Dependent H_2 Adsorption Energies on Cu_xPd_{1-x} Alloy (111) Surfaces. *ACS Catal.* **2015**, *5*, 1020−1026.

DOI: 10.1021/acscatal.8b02168
ACS Catal. 2018, 8, 10486−10497